Research Square

Preprints are preliminary reports that have not undergone peer review.
They should not be considered conclusive, used to inform clinical practice,
or referenced by the media as validated information.

Cuproptosis-related gene signature links immune-metabolic crosstalk to poor prognosis in hepatocellular carcinoma

xin zhang
Second Hospital of Tianjin Medical University
yuhang wang
Tianjin Medical University
mingyang he
Tianjin Medical University
shulei jia
Tianjin Medical University
huijie gao
gaohuijie@tmu.edu.cn
Tianjin Medical University
fang lei
Tianjin Medical University

Research Article

Keywords: Cuproptosis, Hepatocellular carcinoma, Prognostic model, Tumor microenvironment, Immune checkpoints, Drug sensitivity

Posted Date: November 11th, 2026

DOI: https://doi.org/10.21203/rs.3.rs-11330738/v1

License: This work is licensed under a Creative Commons Attribution 4.0 International License.
Read Full License

Additional Declarations: No competing interests reported.

Cuproptosis-related gene signature links immune-metabolic crosstalk to poor prognosis in hepatocellular carcinoma

Xin Zhang[1], Yuhang Wang[1], Mingyang He[2], Shulei Jia[2], Huijie Gao[2*] , and Fang Lei[2*]
1 The Second Hospital Of Tianjin Medical University,Tianjin 300211,China
2 Department of Pathogen Biology, School of Basic Medical Sciences, Tianjin Medical University, Tianjin 300070, China
*** Corresponding author:**
Dr. Huijie Gao, No. 22 Qi-Xiang-Tai Road, Tianjin 300070, China, Tel: +86 22 83336836; Fax: +86 22 83336816; E-mail: gaohuijie@tmu.edu.cn
Dr. Fang Lei, No. 22 Qi-Xiang-Tai Road, Tianjin 300070, China, Tel: +86 22 83336836; Fax: +86 22 83336816; E-mail: leif100@163.com ;

Keywords: Cuproptosis; Hepatocellular carcinoma; Prognostic model; Tumor microenvironment; Immune checkpoints; Drug sensitivity

Abstract

Background: Cuproptosis, a copper-dependent cell death pathway, has emerged as a novel regulatory mechanism in cancer biology. However, the global expression landscape and prognostic value of cuproptosis-related genes in hepatocellular carcinoma (HCC) remain poorly characterized. **Methods:** We systematically analyzed the expression profiles of 18 cuproptosis-related genes using The Cancer Genome Atlas (TCGA) HCC dataset. A prognostic risk model was constructed via LASSO and multivariate Cox regression analyses. Comprehensive bioinformatics analyses were performed to evaluate genomic alterations, functional enrichment, immune infiltration, methylation patterns, and drug sensitivity. Virtual knockout simulations were conducted using scTenifoldKnk to assess gene functions. External validation were performed in the ICGC-LIRI-JP cohort. **Results:** We identified a four-gene prognostic signature (CDKN2A, DLAT, MTF1, and PDHA1) that effectively stratifies HCC patients into high- and low-risk groups, with the risk score serving as an independent prognostic factor. The model genes were significantly enriched in mitochondrial metabolic pathways, including the TCA cycle and pyruvate metabolism, and showed strong associations with immune cell infiltration and immune checkpoint expression. Distinct promoter methylation patterns and differential drug sensitivity profiles were observed across the four genes. Virtual knockout experiments indicated that the four-gene signature acts in concert to modulate both metabolic homeostasis and immune-related pathways in HCC, corroborating the enrichment and immune infiltration findings. External validation indicate that the four-gene signature reproduces its prognostic stratification in an independent RNA-sequencing cohort of HCC.**Conclusion:** Collectively, this study provides the systematic integration of cuproptosis-related genes into a prognostic framework for HCC, offering a novel biomarker panel that may inform individualized risk stratification and precision therapeutic decision-making.

1 Introduction

Hepatocellular carcinoma (HCC) ranks among the most common and deadly cancers worldwide. Despite some progress in prevention, diagnosis, and treatment, most patients

are diagnosed at advanced stages, leading to poor outcomes and a persistently low 5-year survival rate [1, 2]. Current early detection and surveillance rely mainly on ultrasound and serum alpha-fetoprotein (AFP), while newer markers like AFP-L3 and des-gamma-carboxy prothrombin (DCP) need further validation [3, 4]. Imaging and pathology are useful for staging and treatment evaluation, but they suffer from limited sensitivity, invasiveness, or delays. Thus, identifying robust biomarkers for early diagnosis and prognosis is critical to improving HCC management and patient survival [5, 6].

Cuproptosis is a recently recognized form of regulated cell death driven by copper-induced aggregation of mitochondrial lipoylated proteins and loss of iron-sulfur cluster proteins [6]. The liver is central to copper metabolism; under disease conditions, copper overload can trigger oxidative stress, mitochondrial dysfunction, and lipotoxic injury [7, 8]. Several cuproptosis-related genes, including MTF1, ATP7A, and GLS, are differentially expressed in HCC, and expression levels of DLAT, ATP7A, and MTF1 correlate with clinical stage and histological grade [9-11], suggesting a role for copper dysregulation in HCC development. However, a systematic risk model based on copper metabolism-related genes is still lacking, and their regulatory mechanisms and therapeutic potential remain poorly understood. Moreover, how these genes contribute to HCC molecular subtyping, immune microenvironment remodeling, metabolic reprogramming, metastasis, and immune evasion is largely unclear. Therefore, deciphering the molecular network of copper metabolism-related genes in liver cancer may not only refine the theoretical framework of copper-driven tumor promotion but also open new avenues for prognosis and targeted therapy.

Therefore, in this study, we systematically characterized the expression landscape and prognostic value of the copper metabolism-related genes and performing survival and correlation analyses, we constructed and validated a four-gene prognostic risk model (CDKN2A, DLAT, MTF1, PDHA1). We then examined the model's associations with immune infiltration, immune checkpoint molecules, signaling pathways, protein-protein interactions, and immune regulation/evasion, and assessed its sensitivity to commonly used anti-HCC drugs. External validation indicated that the model were reliable. Our findings confirm a significant link between copper metabolism-related genes and HCC prognosis, provide a practical risk model for outcome prediction, and delineate the regulatory network of these four genes in HCC, offering new mechanistic insights and potential targets for copper-targeted HCC therapy.

2 Materials and Methods

2.1 Data acquisition and preprocessing

The mRNA expression profiles and corresponding clinical information of hepatocellular carcinoma (LIHC, also referred to as HCC) samples were retrieved from The Cancer Genome Atlas (TCGA) database (https://portal.gdc.cancer.gov/). RNA-seq data in transcripts per million (TPM) format were $\log_2$-transformed after adding a pseudo-count of 1. Samples with complete transcriptomic and clinical records were retained, yielding a final cohort of 371 HCC cases for subsequent analyses. Differential expression analysis of cuproptosis-related genes was performed using the , with statistical significance defined as adjusted $P < 0.05$ [12].

2.2 GEPIA-based expression and survival analysis

Gene Expression Profiling Interactive Analysis (GEPIA, http://gepia.cancer-pku.cn/) is a web-based tool that integrates TCGA and GTEx datasets for pan-cancer transcriptome interrogation [13]. We employed GEPIA to profile the expression patterns of cuproptosis-related genes in HCC relative to matched normal tissues, with significance set at $P < 0.05$. Survival associations were evaluated using overall survival (OS) metrics, with log-rank $P < 0.05$ considered statistically significant.

2.3 Prognostic model construction

Feature selection for prognostic modeling was performed using Least Absolute Shrinkage and Selection Operator (LASSO) penalized Cox regression, with the optimal regularization parameter (λ) determined via 10-fold cross-validation, with the minimum criterion (λ_{min}) set at 0.0062 [14]. The resulting prognostic risk score was calculated as: $\text{Risk score} = 0.1742 \times \text{CDKN2A} + 0.2766 \times \text{DLAT} + 0.0681 \times \text{MTF1} + 0.049 \times \text{PDHA1}$. All statistical analyses were carried out using R software (version 4.0.3; R Foundation for Statistical Computing) with the glmnet package. P-value < 0.05 was considered statistically significant [15].

2.4 Mutation profiling

Somatic mutation data for the four cuproptosis-related genes were obtained from the cBioPortal database (https://www.cbioportal.org/) [16]. Mutation frequencies were calculated as the percentage of cases harboring non-synonymous alterations, including missense mutations, truncating variants (nonsense and frameshift), and splice-site alterations.

2.5 DNA methylation analysis

Promoter methylation levels of the four genes in HCC were examined using the UALCAN web portal (http://ualcan.path.uab.edu), which integrates TCGA multi-omics data with clinicopathological annotations for stratified analyses of expression and methylation patterns [17].

2.6 Protein–protein interaction network construction

A protein–protein interaction (PPI) network was built using the STRING database (version 12.0, https://string-db.org) [18]. The search was restricted to Homo sapiens, with a minimum interaction score threshold of 0.7 (high confidence). The resulting network was visualized to identify central nodes and potential functional modules associated with the four target genes.

2.7 Functional enrichment analysis

Gene Ontology (GO) term annotation and Kyoto Encyclopedia of Genes and Genomes (KEGG) pathway enrichment analyses were performed on the genes identified in the PPI network [18]. GO analysis covered biological processes, cellular components, and molecular functions, while KEGG analysis focused on metabolic and signaling pathways. Enrichment significance was set at adjusted $P < 0.05$. The GO resource was accessed via http://geneontology.org, and KEGG via https://www.genome.jp/kegg/.

2.8 Subcellular localization analysis

The subcellular localization data of the four proteins encoded by the gene signature were retrieved from the Human Protein Atlas (HPA) database.

2.9 Immune landscape characterization

To evaluate the association between the four-gene signature and tumor-infiltrating immune cells, we analyzed immune cell abundance using the TIMER 2.0 platform (https://timer.cistrome.org) [19], which provides tissue-specific deconvolution of immune

cell types from bulk transcriptomic data. Correlations between gene expression and infiltration levels of B cells, $CD4^+$ T cells, $CD8^+$ T cells, macrophages, neutrophils, and dendritic cells were computed, with $P < 0.05$ considered significant. In parallel, we assessed the expression correlations of the four genes with a panel of immune checkpoint molecules, including PDCD1, CD274, CTLA4, LAG3, HAVCR2, PDCD1LG2, TIGIT, and SIGLEC15, using the same statistical threshold.

2.10 Drug sensitivity prediction

Drug response associations were interrogated using two pharmacogenomic databases: the Genomics of Drug Sensitivity in Cancer (GDSC, https://www.cancerrxgene.org/) and the Cancer Therapeutics Response Portal (CTRP, https://portals.broadinstitute.org/ctrp). For each gene, Spearman correlation coefficients were computed between expression levels and drug sensitivity metrics (e.g., IC_{50} or AUC), with significance defined as $|R| > 0.2$ ($P < 0.05$) for GDSC and $|R| > 0.15$ ($P < 0.05$) for CTRP.

2.11 Virtual knockout of the four-gene signature in HCC

To functionally validate the regulatory roles of the four-gene signature (CDKN2A, DLAT, MTF1, and PDHA1), we performed in silico combinatorial gene knockout simulations using the scTenifoldKnk framework. Single-cell RNA-sequencing data in .h5 format and corresponding cell-type annotations were obtained from the TISCH database [20]. Preprocessing, quality control, and downstream analysis were carried out with the R packages MAESTRO and Seurat, followed by re-clustering of cells via t-SNE to define homogeneous subpopulations.

scTenifoldKnk extends the scTenifoldNet algorithm to model perturbation effects on cell-specific regulatory networks [21]. In brief, it constructs a multi-layer gene regulatory network for the baseline condition by applying tensor decomposition across transcriptionally similar cell groups. To simulate gene knockout, the expression of the target gene(s) was forced to zero, and the perturbed network was rebuilt while preserving the original data structure. By comparing the adjacency matrices of the wild-type and perturbed networks, we calculated Z-scores and $\log_2$ fold changes ($\log_2$FC) for each gene, reflecting the magnitude of regulatory rewiring induced by the knockout. Statistical significance was assessed using adjusted p-values with Benjamini–Hochberg correction to control the false discovery rate (FDR). For the combined knockout, CDKN2A, DLAT, MTF1, and PDHA1 were simultaneously zeroed; the top 20 genes exhibiting the most pronounced transcriptional changes were selected for subsequent functional characterization.

2.12 External validation

To assess the reproducibility of the four-gene signature, we performed external validation in the ICGC-LIRI-JP (Liver Cancer - RIKEN, Japan) cohort, an independent RNA-sequencing dataset of hepatocellular carcinoma [22]. Gene-level expression data and corresponding clinical annotations were retrieved from the HCCDB resource [23]. After restricting to primary tumour samples with available overall survival (OS) information and retaining one sample per patient, 203 patients were eligible (35 deaths; median follow-up, 27.0 months). Risk scores were calculated by applying the coefficients of the originally constructed model -- $\text{Risk score} = 0.1742 \times \text{CDKN2A} + 0.2766 \times \text{DLAT} + 0.0681 \times \text{MTF1} + 0.049 \times \text{PDHA1}$ -- to the expression values of the validation cohort, without refitting any parameter. Patients were dichotomized at the

cohort median risk score. OS was compared between risk groups using Kaplan-Meier estimates and the log-rank test. Time-dependent areas under the receiver operating characteristic curve (AUCs) were computed at 12 and 36 months using the timeROC package. Cox proportional-hazards models were used to estimate hazard ratios (HRs) with 95% confidence intervals (CIs); the multivariable model was adjusted for age, sex, and T stage. The proportional-hazards assumption was verified with scaled Schoenfeld residuals. Discrimination was summarized by Harrell's C-index, and estimate stability was assessed by bootstrap resampling (1,000 replicates).

2.13 Statistical analysis

All statistical computations were performed using the built-in functions of the respective online databases and R/Python environments described above. Continuous variables were compared using appropriate parametric or non-parametric tests as indicated. Correlation analyses were based on Spearman’s rank correlation. Survival differences were assessed by Kaplan–Meier curves with log-rank tests. Unless otherwise specified, a two-sided $P < 0.05$ was considered statistically significant. All reported P-values were nominal without adjustment unless noted (e.g., FDR correction for scRNA-seq perturbation analyses).

3 Results

3.1 Expression profiles of cuproptosis--related genes in HCC

To systematically characterize the transcriptional landscape of cuproptosis-related genes in hepatocellular carcinoma (HCC), we interrogated the RNA-sequencing data from The Cancer Genome Atlas (TCGA) for a curated panel of 18 core regulatory genes, including NFE2L2, NLRP3, ATP7B, ATP7A, SLC31A1, FDX1, LIAS, LIPT2, DLD, DLAT, PDHA1, PDHB, MTF1, GLS, CDKN2A, DBT, GCSH, and DLST. Differential expression analysis between HCC specimens and adjacent non-tumor tissues revealed a marked dichotomy in the dysregulation patterns of these transcripts. Specifically, 11 genes—ATP7A, LIAS, LIPT2, DLD, DLAT, PDHA1, PDHB, MTF1, GLS, CDKN2A, and DLST—exhibited significantly elevated expression levels in tumor samples, whereas NFE2L2, ATP7B, SLC31A1, DBT, and GCSH showed substantially reduced transcript abundances (all $P < 0.05$) (Figure 1A-1R).

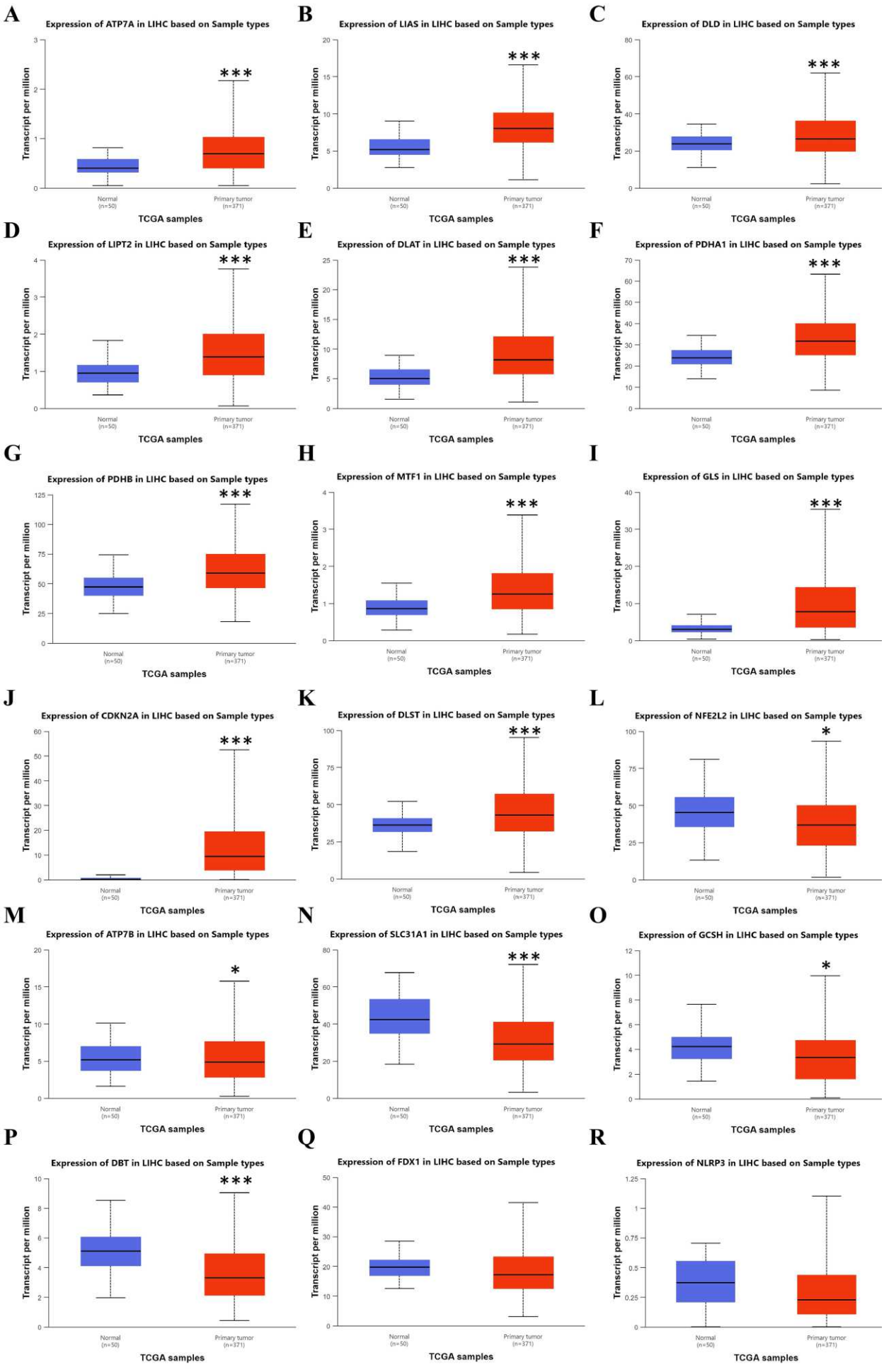

A
Expression of ATP7A in LIHC based on Sample types
B
Expression of LIAS in LIHC based on Sample types
C
Expression of DLD in LIHC based on Sample types
D
Expression of LIPT2 in LIHC based on Sample types
E
Expression of DLAT in LIHC based on Sample types
F
Expression of PDHA1 in LIHC based on Sample types
G
Expression of PDHB in LIHC based on Sample types
H
Expression of MTF1 in LIHC based on Sample types
I
Expression of GLS in LIHC based on Sample types
J
Expression of CDKN2A in LIHC based on Sample types
K
Expression of DLST in LIHC based on Sample types
L
Expression of NFE2L2 in LIHC based on Sample types
M
Expression of ATP7B in LIHC based on Sample types
N
Expression of SLC31A1 in LIHC based on Sample types
O
Expression of GCSH in LIHC based on Sample types
P
Expression of DBT in LIHC based on Sample types
Q
Expression of FDX1 in LIHC based on Sample types
R
Expression of NLRP3 in LIHC based on Sample types
Transcript per million
Normal (n=50)
Primary tumor (n=371)
TCGA samples

Figure 1. Expression profiles of 18 cuproptosis-related genes in normal and HCC tissues. RNA expression levels of ATP7A (A), LIAS (B), DLD (C), LIPT2 (D), DLAT (E), PDHA1 (F), PDHB (G), MTF1 (H), GLS (I), CDKN2A (J), DLST (K), NFE2L2 (L), ATP7B (M), SLC31A1 (N), GCSH (O), DBT (P), FDX1 (Q), and NLRP3 (R) in HCC tissues were analyzed using TCGA datasets. *P < 0.05; **P < 0.001.

In contrast, the expression levels of NLRP3 and FDX1 remained statistically comparable between the two groups, suggesting their relative insensitivity to the malignant transformation process in HCC.

3.2 Prognostic values of cuproptosis-related genes in HCC

To translate these expression aberrations into clinically relevant prognostic information, we next evaluated the association between the 18 cuproptosis-related genes and patient survival outcomes. Using the UALCAN database, we performed Kaplan–Meier survival analyses with log-rank tests, stratifying HCC patients according to the median expression level of each individual gene. Among the upregulated candidates, only four—CDKN2A, DLAT, MTF1, and PDHA1—demonstrated a statistically significant correlation with poorer overall survival (OS), each yielding a log-rank P < 0.05 (Figure 2A-2R).

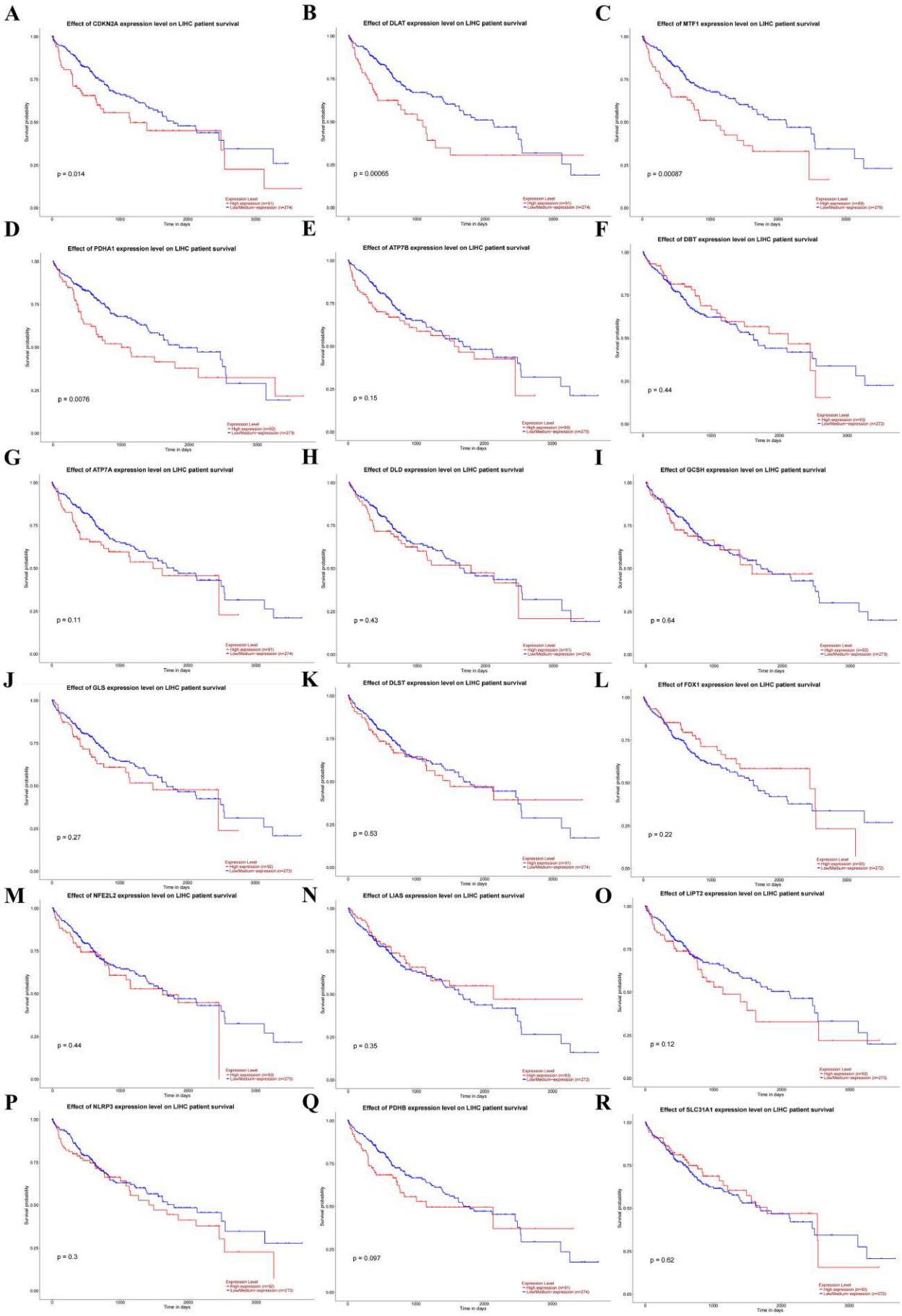


Figure 2. Prognostic significance of the four cuproptosis-related genes in HCC. Kaplan–Meier survival curves for overall survival (OS) stratified by the expression levels

of CDKN2A (A), DLAT (B), MTF1 (C), PDHA1 (D), ATP7B (E), DBT (F), ATP7A (G), DLD (H), GCSH (I), GLS (J), DLST (K), FDX1 (L), NFE2L2 (M), LIAS (N), LIPT2 (O), NLRP3 (P), PDHB (Q), and SLC31A1 (R) in HCC patients based on the UALCAN database. The log-rank P-value is indicated for each comparison. $P < 0.05$ was considered statistically significant.

These findings indicate that while a substantial proportion of cuproptosis-related genes are transcriptionally activated in HCC, only a distinct subset may serve as clinically meaningful predictors of unfavorable prognosis, potentially guiding risk stratification in this patient population.

3.3 A prognostic model based on four cuproptosis-related genes in HCC

To translate the prognostic significance of the four candidate genes into a clinically applicable risk stratification framework, we constructed a multi-gene risk signature based on the expression levels of CDKN2A, DLAT, MTF1, and PDHA1. The risk score for each individual patient was computed as a linear combination of the respective transcript abundances, weighted by the regression coefficients derived from multivariate Cox proportional-hazards modeling. Upon stratification of the entire HCC cohort according to the median risk score, patients were dichotomized into high- and low-risk groups. Kaplan–Meier survival analysis demonstrated that individuals in the high-risk group exhibited markedly shorter overall survival (OS) and consistently lower survival probabilities across the follow-up period, relative to their low-risk counterparts (log-rank $P < 0.01$; hazard ratio [HR] = 1.682, 95% confidence interval [CI]: 1.187–2.383) (Figure 3A-3E).

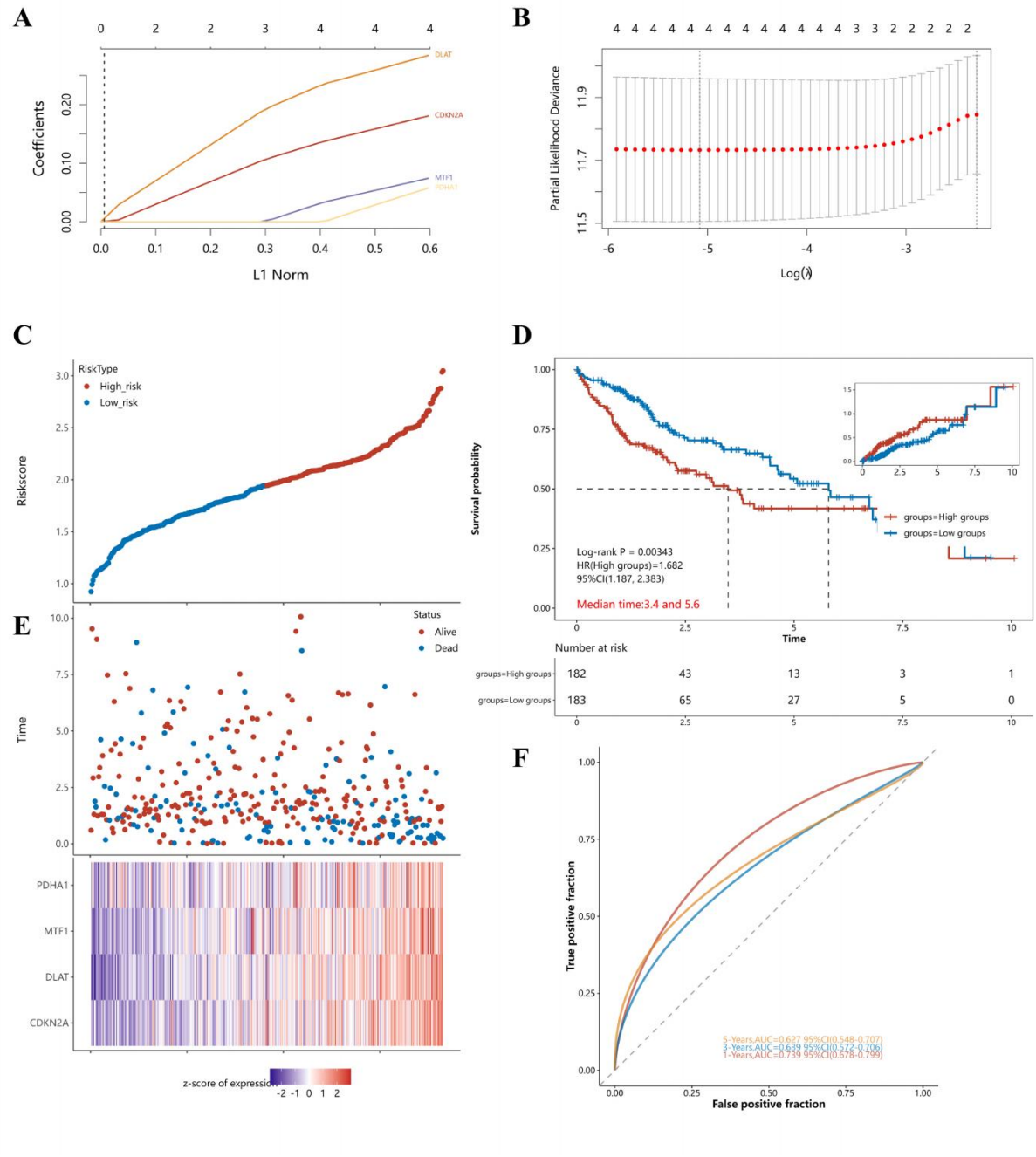


Figure 3. Construction and evaluation of the four-gene prognostic risk model in HCC. (A) LASSO coefficient profiles of the selected genes as a function of the log(λ) penalty parameter. (B) Partial likelihood deviance versus log(λ) with 10-fold cross-validation. (C) Risk score distribution of HCC patients ranked from low to high risk, with color coding indicating high- and low-risk groups. (D) Kaplan–Meier survival analysis comparing OS between high- and low-risk groups. (E) Survival time and status distribution of patients in each risk group, with the corresponding heatmap showing the expression patterns of the four signature genes. (F) Time-dependent receiver operating characteristic (ROC) curves for predicting 1-, 3-, and 5-year OS. Log-rank P < 0.05 was considered statistically significant.

To further validate the discriminative capacity of this signature, we performed time-dependent receiver operating characteristic (ROC) curve analyses. The area under

the curve (AUC) values for OS at 1, 3, and 5 years were 0.739, 0.639, and 0.627, respectively (Figure 3F), indicating satisfactory short-term predictive performance with a gradual attenuation in long-term prognostic accuracy. Collectively, these results suggest that the four-gene signature serves as a robust and independent stratification tool, effectively distinguishing HCC patients with divergent clinical trajectories and holding promise for guiding individualized prognostic assessment.

3.4 Mutational landscape of the four cuproptosis-related genes in HCC.

To further delineate the genomic underpinnings of the four prognostic candidates, we systematically interrogated the cBioPortal database to comprehensively evaluate their mutational frequencies, variant classification spectra, and structural alteration patterns in HCC. Among the four genes, CDKN2A exhibited the highest mutational burden, with an overall alteration frequency of 9%, substantially outpacing PDHA1 (0.8%), MTF1 (0.6%), and DLAT (0.5%). At the variant-type level, missense mutations emerged as the most prevalent category across the gene set (Figure S1). However, a closer examination of the alteration spectra revealed a striking dichotomy in their molecular characteristics: whereas PDHA1, MTF1, and DLAT were predominantly characterized by nucleotide substitutions, CDKN2A displayed a distinctly divergent and biologically consequential alteration profile, driven chiefly by deep deletions and truncating mutations rather than missense events. Collectively, these mutational signatures highlight the genetic heterogeneity among the four genes in HCC.

3.5 Correlations between four cuproptosis-related genes and cell signaling pathways in HCC

To explore the biological pathways potentially associated with the four prognostic genes, we performed Gene Ontology (GO) and Kyoto Encyclopedia of Genes and Genomes (KEGG) enrichment analyses. KEGG analysis revealed significant enrichment in pathways related to the citrate cycle (TCA cycle), carbon metabolism, propanoate metabolism, valine, leucine and isoleucine degradation, pyruvate metabolism, glycolysis/gluconeogenesis, lipoic acid metabolism, metabolic pathways, central carbon metabolism in cancer, and glyoxylate and dicarboxylate metabolism (Figure 4A).

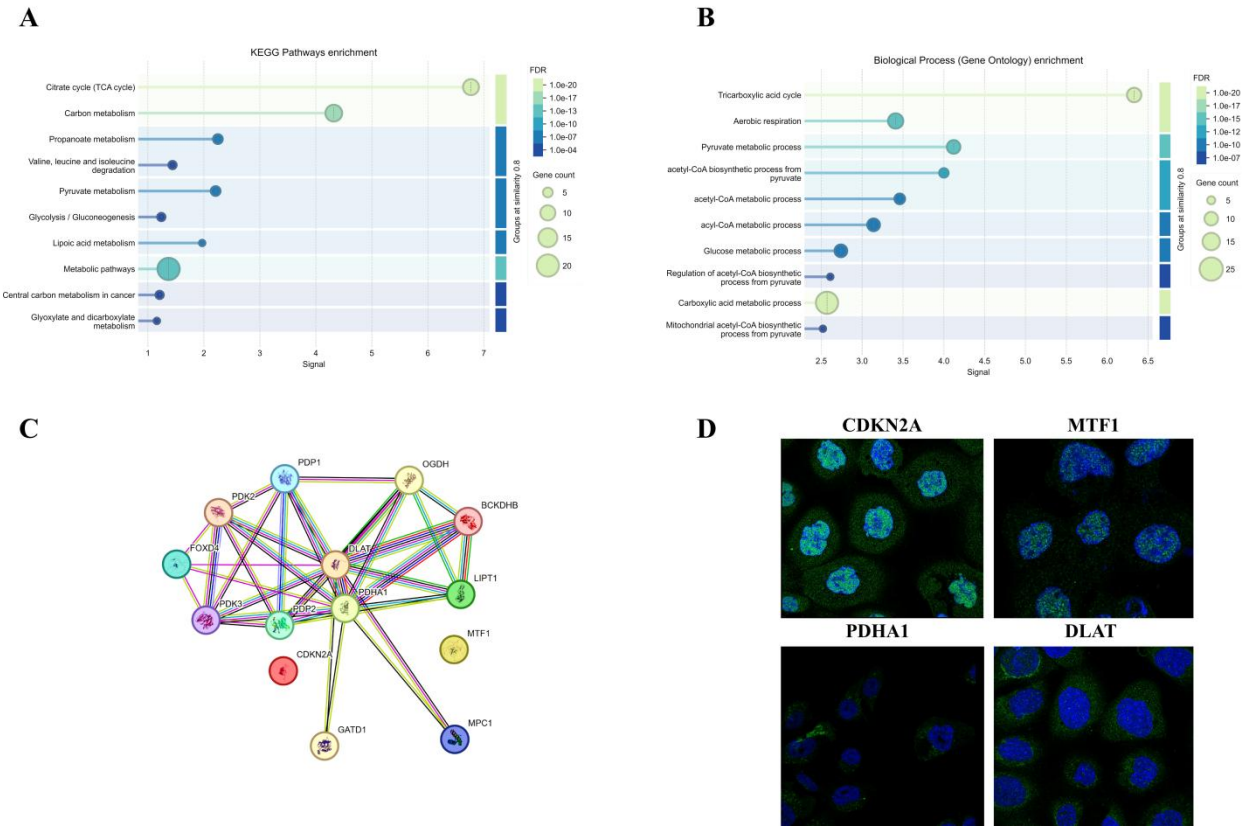


Figure 4. Functional enrichment and protein interaction network of the four-gene signature. (A) KEGG pathway enrichment analysis of the four cuproptosis-related genes. (B) GO biological process enrichment analysis. (C) Protein–protein interaction (PPI) network constructed using the STRING database, with edge thickness indicating confidence scores. (D) Subcellular localization of the four proteins based on the Human Protein Atlas (HPA) database.

GO enrichment analysis identified significant overrepresentation of biological processes involved in the tricarboxylic acid cycle, aerobic respiration, pyruvate metabolic process, acetyl-CoA biosynthetic process from pyruvate, acetyl-CoA metabolic process, acyl-CoA metabolic process, glucose metabolic process, regulation of acetyl-CoA biosynthetic process from pyruvate, carboxylic acid metabolic process, and mitochondrial acetyl-CoA biosynthetic process from pyruvate (Figure 4B).

Furthermore, a protein-protein interaction (PPI) network was constructed using the STRING database. The network comprised 14 nodes and 35 edges, with an average local clustering coefficient of 0.71 ($P < 0.001$) (Figure 4C), indicating significant interconnectivity among DLAT, PDHA1, and several other mitochondrial enzyme-encoding genes, including PDP1, PDK2, FOXD4, PDK3, PDP2, OGDH, BCKDHB, LIPT1, GATD1, and MPC1. In contrast, CDKN2A and MTF1 appeared as separate nodes without any direct connections to DLAT or PDHA1 within the network. To investigate this connectivity disparity, we retrieved subcellular localization annotations for the four proteins. CDKN2A and MTF1 are exclusively localized to the nucleoplasm, whereas PDHA1 and DLAT are confined to the mitochondrial matrix and intermembrane space (Figure 4D). Collectively, these results suggest that the four genes are associated with metabolic pathways, particularly those related to the TCA cycle and pyruvate metabolism, and that DLAT and PDHA1 may functionally interact with multiple

mitochondrial enzyme-coding genes, whereas CDKN2A and MTF1 exhibit no direct connectivity to these interactions within the PPI network, consistent with their distinct subcellular compartmentalization.

3.6 Association of the four-gene risk signature with immune cell infiltration and immune checkpoints in HCC

To investigate the relationship between the four-gene signature and the tumor immune microenvironment, we evaluated the correlations between the expression of the four genes and the infiltration abundances of six major immune cell types using the TIMER database. CDKN2A, DLAT, MTF1, and PDHA1 all exhibited significantly positive correlations with the infiltration levels of B cells, $CD8^+$ T cells, $CD4^+$ T cells, macrophages, neutrophils, and dendritic cells (Figure 5A-5D).

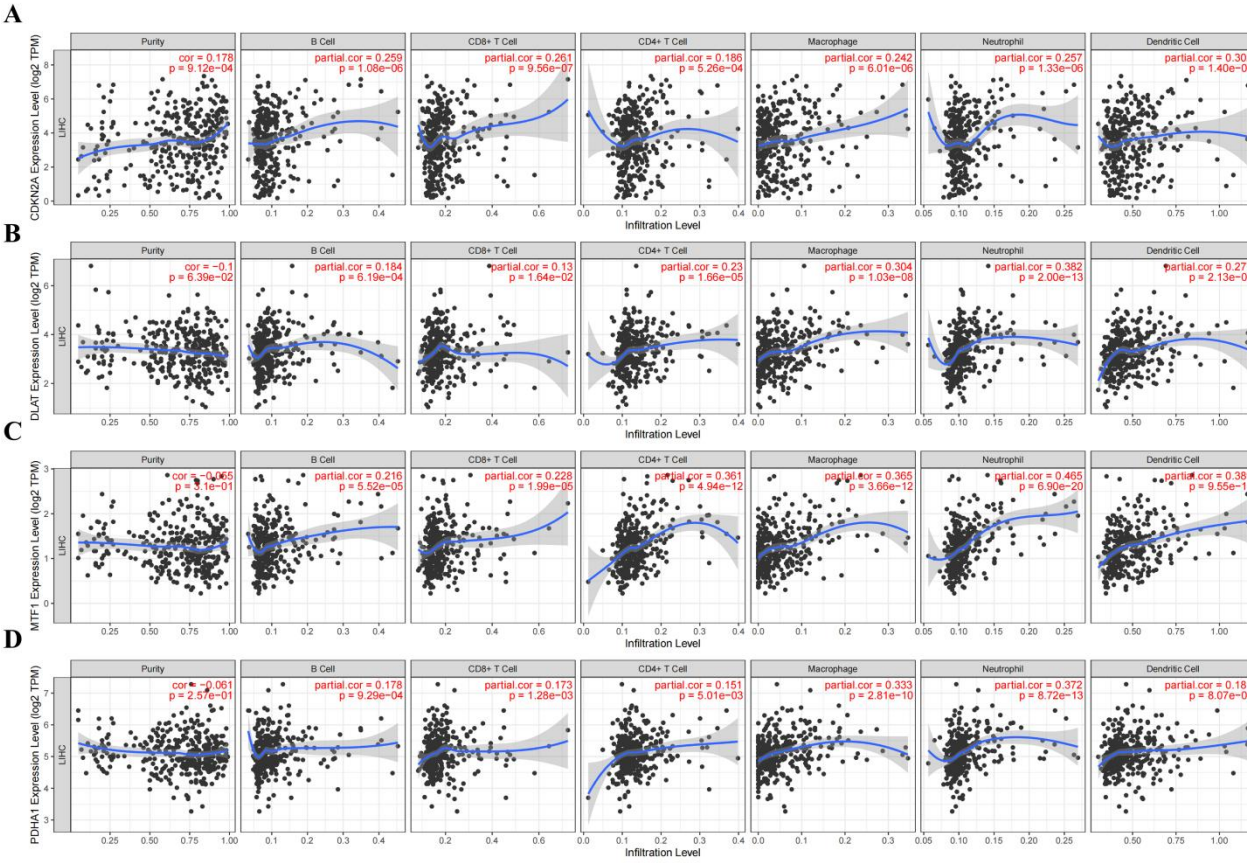


Figure 5. Correlations between the four-gene signature and immune cell infiltration in HCC. Scatter plots showing the associations between the expression levels of CDKN2A (A), DLAT (B), MTF1 (C), and PDHA1 (D) and the infiltration abundances of B cells, $CD8^+$ T cells, $CD4^+$ T cells, macrophages, neutrophils, and dendritic cells in HCC based on the TIMER database. Spearman correlation coefficients and P-values are shown. $P < 0.05$ was considered statistically significant.

To further explore the immunomodulatory associations of the four genes, we assessed their expression correlations with a panel of established immune checkpoint genes, including PDCD1, CD274, CTLA4, LAG3, HAVCR2, TIGIT, and SIGLEC15. Correlation analysis revealed that CDKN2A was significantly positively correlated with PDCD1, CTLA4, CD274, HAVCR2, LAG3, PDCD1LG2, and TIGIT; DLAT with CD274, HAVCR2, LAG3, PDCD1LG2, and TIGIT; MTF1 with CTLA4, CD274, HAVCR2, PDCD1LG2, and TIGIT; and PDHA1 with CD274, HAVCR2, and PDCD1LG2 (Figure S2). Collectively,

these results suggest that the four genes are positively associated with the infiltration of multiple immune cell types and the expression of most examined immune checkpoint genes in HCC.

3.7 Prediction of upstream methylation of four cuproptosis-related genes

To explore the potential epigenetic regulation of the four genes in HCC, we analyzed their promoter methylation levels using the UALCAN database. Compared with normal controls, HCC tissues exhibited significantly lower promoter methylation levels of DLAT and MTF1, whereas CDKN2A showed significantly higher promoter methylation levels (Figure 6A-6C).

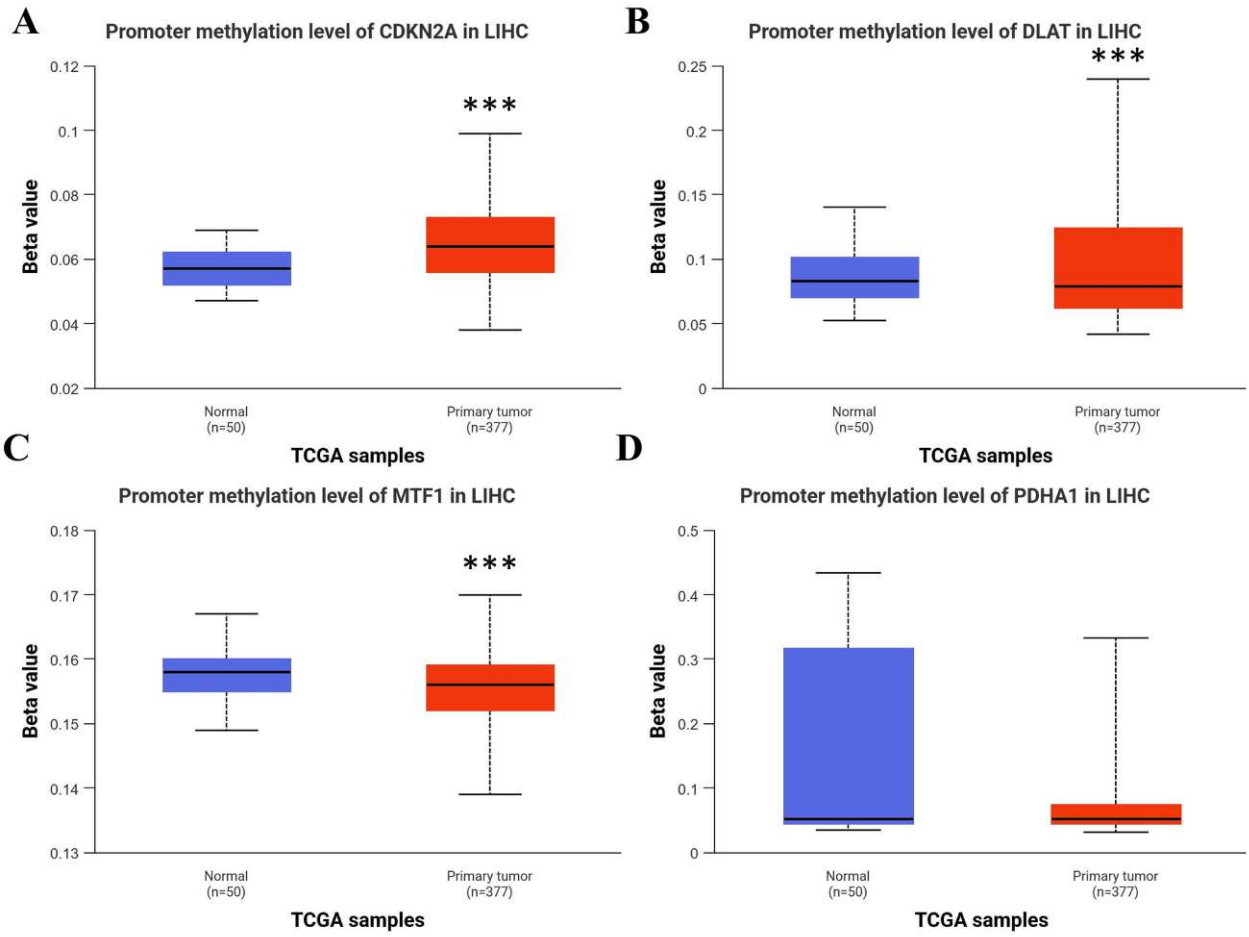


Figure 6. Promoter methylation profiles of the four cuproptosis-related genes in HCC. Box plots comparing promoter methylation levels between HCC and normal tissues for CDKN2A (A), DLAT (B), MTF1 (C), and PDHA1 (D) based on the UALCAN database. ***P < 0.001.

No significant difference was observed for PDHA1 (Figure 6D). Collectively, these results suggest that DLAT and MTF1 display distinct hypomethylation patterns, while CDKN2A is characterized by hypermethylation in HCC, with PDHA1 showing no significant methylation alteration.

3.8 Drug sensitivity prediction of four cuproptosis-related genes in HCC

To evaluate the potential association between the four-gene signature and chemotherapeutic sensitivity, we analyzed drug response data from the Genomics of Drug Sensitivity in Cancer (GDSC) and Cancer Therapeutics Response Portal (CTRP) databases. In the GDSC dataset, high expression of the four-gene signature was

associated with increased sensitivity to NPK76-II-72-1, and resistance to PD-0332991,Nutlin-3a and TGX221 (|R| > 0.2, P < 0.05) (Figure 7A).

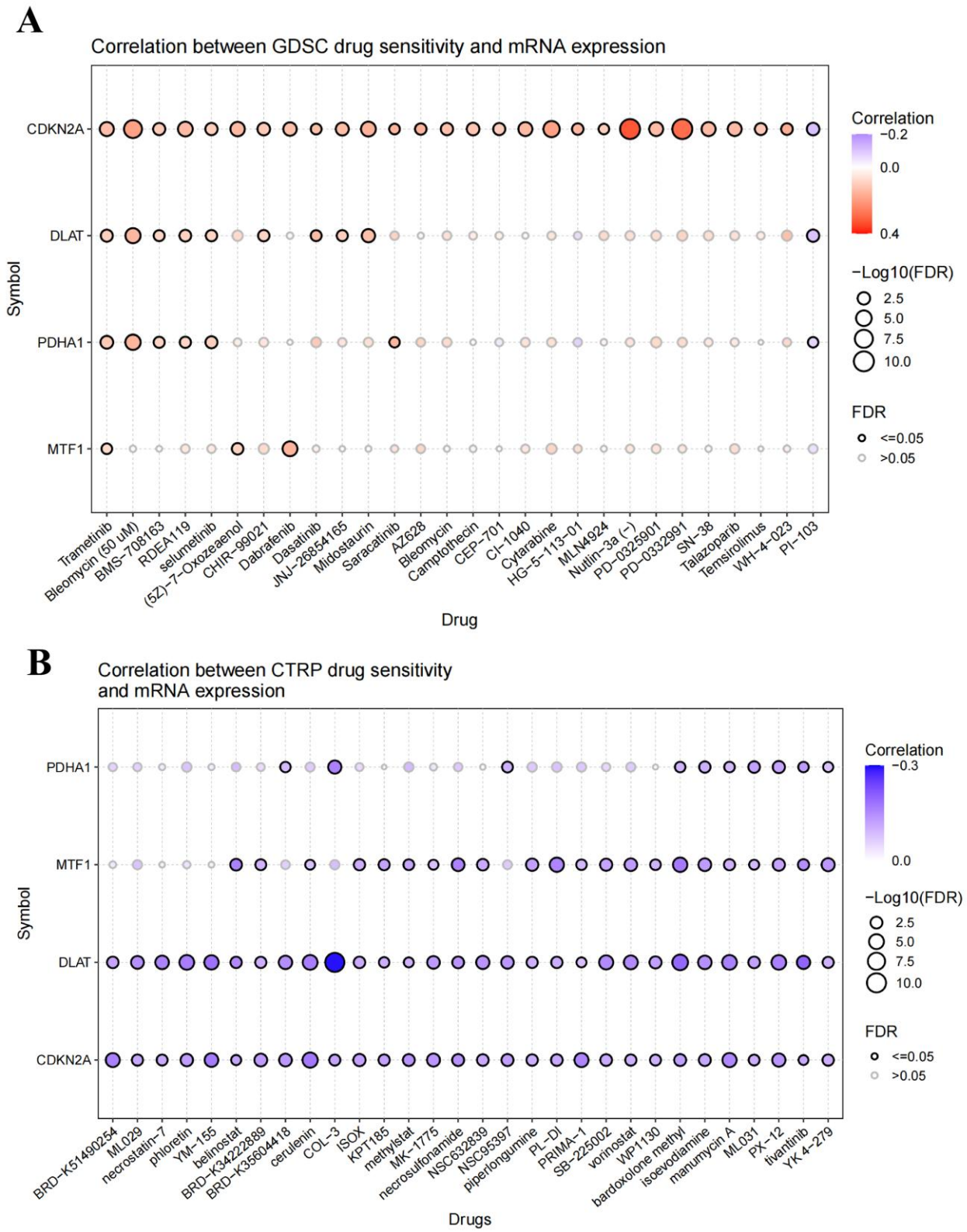


Figure 7. Drug sensitivity prediction based on the four-gene signature. Predicted drug responses associated with the expression of the four-gene signature in pan-cancer datasets from the GDSC (A) and CTRP (B) databases. Red indicates higher sensitivity, and blue indicates higher resistance (|R| > 0.2 for GDSC, |R| > 0.15 for CTRP; P < 0.05). Detailed drug names are listed in Supplementary Table S1 and S2.

In the CTRP dataset, high expression of the four-gene signature was associated with increased sensitivity to a panel of 12 compounds, including tozasertib, COL-3, ciclopirox, MI-2, methotrexate, valdecoxib, PF-750, cytarabine hydrochloride, SR-II-138A, BRD-K97651142, GW-405833, and tivantinib ($|R| > 0.15$, $P < 0.05$), with no resistance associations identified (Figure 7B). Notably, no overlapping compounds were observed between the two datasets, except for the apparent discordance regarding cytarabine—which was predicted as a resistance agent in GDSC but its hydrochloride form showed sensitivity in CTRP. Collectively, these results suggest that the four-gene signature is associated with distinct drug sensitivity profiles across different pharmacological databases, with broader sensitivity predictions in CTRP and a more limited, resistance-inclined profile in GDSC.

3.9 Verification of the four-gene signature functions via virtual knockout in HCC

To functionally validate the regulatory roles of the four-gene signature in HCC, we performed virtual knockout simulations using scTenifoldKnk and identified the top 20 genes with the most significant transcriptional alterations following combinatorial perturbation of all four genes (Figure 8A-8B).

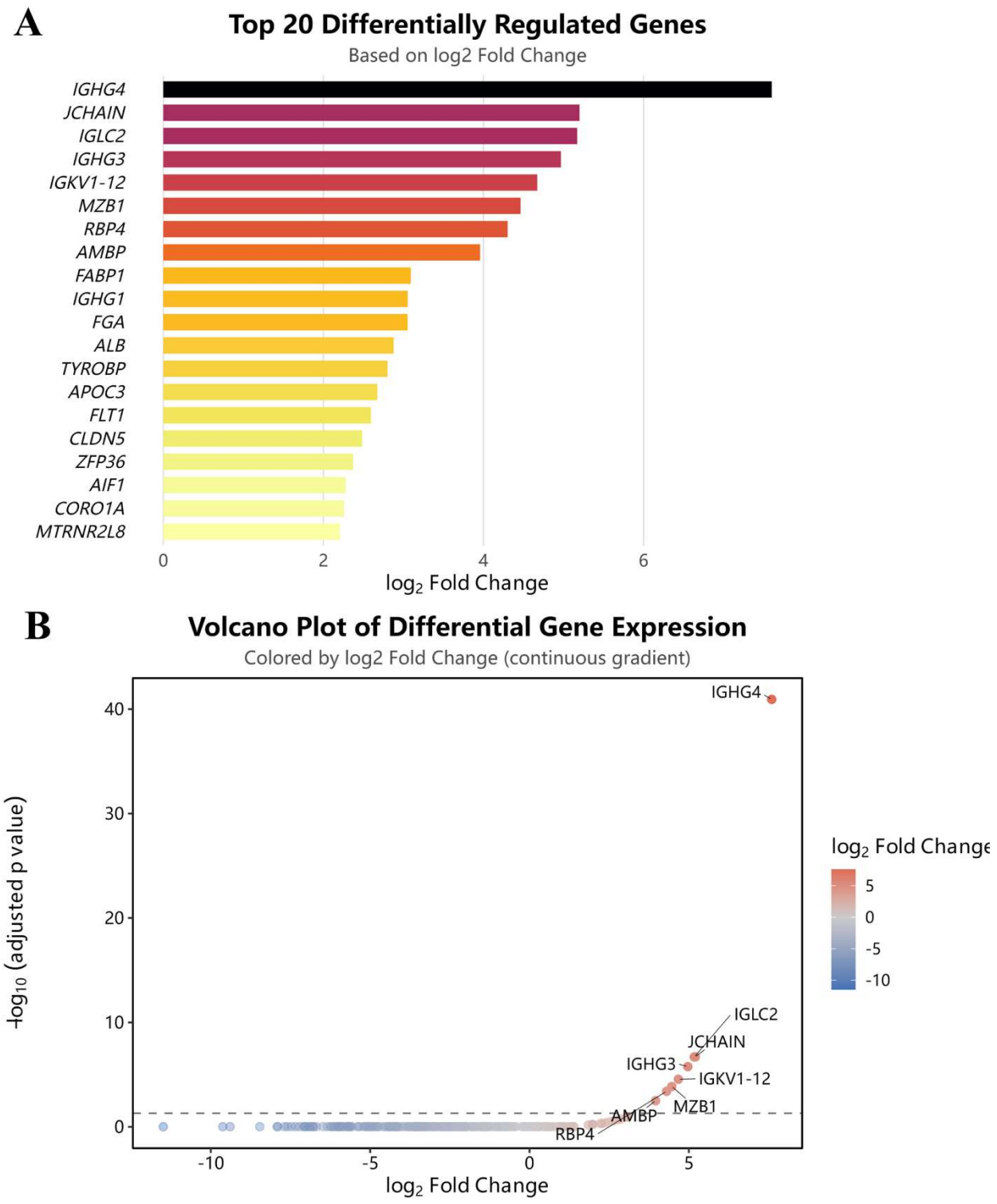


Figure 8. Virtual knockout validation of the four-gene signature in HCC. (A) Top 20 differentially expressed genes following combinatorial virtual knockout of the four signature genes using scTenifoldKnk. (B) Volcano plot depicting the overall transcriptional changes induced by combinatorial perturbation. Red and blue dots represent significantly upregulated and downregulated genes, respectively ($log_2FC > 0.5$, adjusted $P < 0.05$).

Among the top 20 differentially affected genes, those related to immunoglobulin production and B-cell activation—including IGHG3, IGLC2, IGKV1-12, JCHAIN, and

MZB1—were predominantly upregulated. Genes involved in hepatic metabolic functions, such as ALB, RBP4, AMBP, APOC3, and FGA, exhibited downregulation. In addition, immune-related genes (TYROBP, AIF1, CORO1A, and ZFP36) and genes involved in tight junction (CLDN5), fatty acid transport (FABP1), and mitochondrial signaling (MTRNR2L8) also showed significant changes. Collectively, these results suggest that the four-gene signature may act in concert to modulate both metabolic homeostasis and immune-related pathways in HCC, consistent with the enrichment and immune infiltration findings described above.

3.10 External validation of the four-gene signature in an independent RNA-sequencing cohort

We next examined whether the prognostic performance of the four-gene signature was reproducible in an independent cohort. Applying the original coefficients to the ICGC-LIRI-JP cohort (n = 203; 35 deaths), patients in the high-risk group had significantly shorter OS than those in the low-risk group (log-rank P = 0.0002; Figure 9C).

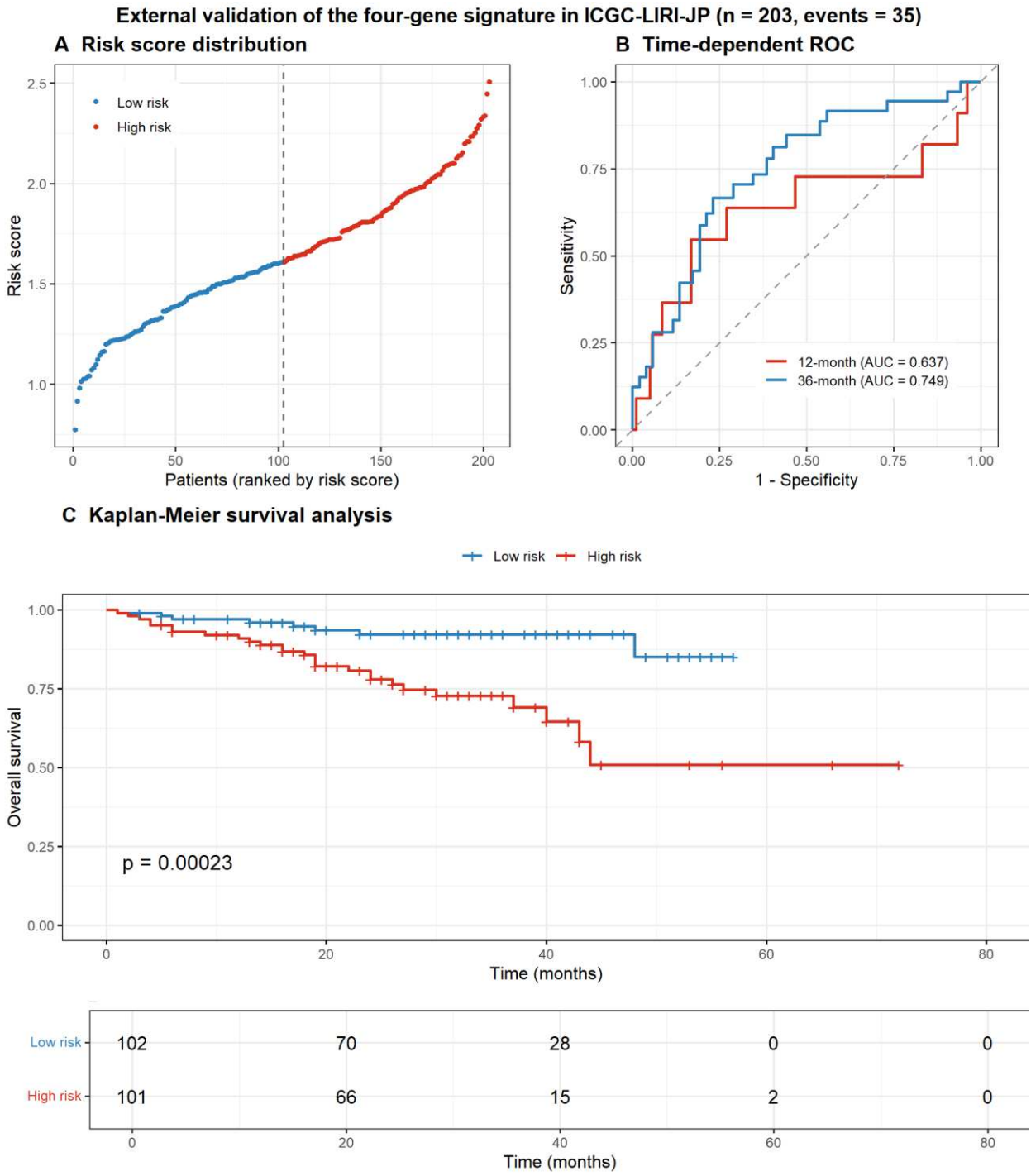


Figure 9. External validation of the four-gene prognostic signature in the ICGC-LIRI-JP cohort (n = 203; 35 deaths). (A) Distribution of risk scores, with patients ranked by risk score and dichotomized at the median (dashed line). (B) Time-dependent ROC curves for 12-month and 36-month overall survival. (C) Kaplan-Meier curves for overall survival in the high- and low-risk groups, with the number of patients at risk shown below. P value was calculated by the log-rank test.

The risk score was associated with a 4.01-fold increased risk of death (HR = 4.01, 95% CI 1.81-8.88, P = 0.0006), corresponding to an HR of 2.04 (95% CI 1.43-2.90) per standard-deviation increase. The association remained significant after adjustment for age, sex, and T stage (HR = 4.51, 95% CI 1.57-12.97, P = 0.005). The signature showed

moderate discriminative ability, with time-dependent AUCs of 0.637 and 0.749 at 12 and 36 months, respectively, and a C-index of 0.687 (Figure 9A-9B). The proportional-hazards assumption was satisfied (P = 0.959), and the direction of the association was consistent across 1,000 bootstrap resamples. These results indicate that the four-gene signature reproduces its prognostic stratification in an independent RNA-sequencing cohort of HCC.

4 Discussion

Cuproptosis, as a novel form of regulated cell death, has garnered considerable attention due to its unique copper-dependent regulatory mechanisms. Given that the liver serves as the central organ for systemic copper metabolism, the interplay between cuproptosis and hepatocarcinogenesis has emerged as a topic of intensive investigation [9-11]. Although previous studies have identified several cuproptosis-related genes—such as DLAT and FDX1—as participants in the regulation of cell migration, proliferation, and drug responsiveness in HCC [24-30], and although targeting cuproptosis pathways holds therapeutic promise [31-33], a systematic evaluation of the global expression landscape of cuproptosis-related genes and their utility as prognostic biomarkers in HCC has remained lacking. This knowledge gap has constrained the clinical application of cuproptosis-related genes in stratified management of HCC.

To address this gap, we systematically profiled the expression of cuproptosis-related genes in HCC and constructed a multi-gene prognostic risk model comprising CDKN2A, DLAT, MTF1, and PDHA1. This signature effectively stratified HCC patients into high- and low-risk groups, with the high-risk cohort exhibiting markedly shorter overall survival. Multivariate Cox regression analysis further confirmed the risk score as an independent prognostic factor in HCC. These findings suggest that coordinated dysregulation of cuproptosis-related genes—rather than alterations of individual genes—may play a more critical role in driving HCC progression. The model provides clinicians with a quantitative tool for outcome prediction and individualized surveillance planning, while also indirectly implicating copper metabolic disturbance as a potentially important microenvironmental contributor to HCC aggressiveness.

Previous studies on CDKN2A, DLAT, MTF1, and PDHA1 in HCC have largely been fragmented single-gene reports focusing on their respective molecular functions [24, 34-40]. CDKN2A is significantly overexpressed in HCC tissues, and its high expression correlates closely with tumor size, clinical stage, and poor prognosis, having been validated as an independent risk factor [34]. Mechanistically, CDKN2A may drive HCC progression through cell-cycle regulation and immune microenvironment modulation, including enhanced dendritic cell and Th2 cell infiltration alongside reduced $CD8^+$ T and NK cell recruitment [35]. DLAT, a key cuproptosis effector, is also upregulated in HCC and associated with adverse outcomes. It suppresses leucine catabolism via AUH acetylation to activate mTOR signaling, and promotes epithelial–mesenchymal transition (EMT) and HCC metastasis through GLUT1-mediated aerobic glycolysis [24, 36]. MTF1, a zinc-dependent transcription factor, promotes HCC cell proliferation when overexpressed and correlates with poor prognosis, whereas its knockdown suppresses proliferation, invasion, and migration while elevating reactive oxygen species levels and promoting cell death [37, 38]. PDHA1 is significantly upregulated in HCC and linked to unfavorable clinical outcomes [40]. It interacts with the long non-coding RNA LINC00607

to synergistically promote HCC cell proliferation and migration, while also enhancing PD-L1 expression to facilitate immune evasion [39]. Collectively, these four genes exhibit pro-tumorigenic expression patterns and prognostic significance in HCC, albeit with distinct mechanistic emphases—CDKN2A primarily in cell-cycle and immune regulation, DLAT in metabolic reprogramming and EMT, MTF1 as a transcriptional regulator of downstream targets, and PDHA1 in both metabolic control and immune escape. These observations provide a robust biological rationale for the four-gene signature. Nevertheless, none of these studies have addressed whether coordinated dysregulation of these core cuproptosis pathway members more accurately reflects HCC malignancy at the systems level, and no prior investigation has integrated them into a multi-gene prognostic model with systematic assessment of its independent prognostic value in HCC risk stratification.

The present study represents the first attempt to incorporate these four cuproptosis-related genes into a unified prognostic model, overcoming the fragmentation inherent in single-gene approaches. Unlike previous studies that merely correlated individual gene expression with prognosis, our multivariate Cox regression analysis demonstrates that the four-gene risk score is an independent prognosticator beyond conventional clinicopathological variables. This finding highlights that synergistic effects among cuproptosis-related genes may exert a more decisive influence on HCC progression than isolated gene dysregulation, and the establishment of this model provides a theoretical foundation for future investigations into how multi-gene interactions within the cuproptosis pathway collectively drive malignant phenotypes in HCC.

To further elucidate the biological underpinnings of this prognostic signature, we examined the genomic alteration patterns and pathway enrichment characteristics of the four genes. CDKN2A exhibited a substantially higher mutation frequency (9%) compared with the other three genes, predominantly characterized by deep deletions and truncating mutations, whereas PDHA1 (0.8%), MTF1 (0.6%), and DLAT (0.5%) were primarily affected by missense substitutions, indicating marked mutational heterogeneity among the four genes. Functional enrichment analysis revealed significant co-enrichment in mitochondrial core metabolic pathways, including the TCA cycle, pyruvate metabolism, and acetyl-CoA biosynthesis. Protein–protein interaction analysis further confirmed that DLAT and PDHA1 engage in direct or indirect interactions with multiple mitochondrial enzyme-encoding genes. This convergent enrichment pattern is particularly intriguing, given that cuproptosis is initiated by the direct binding of copper to lipoylated proteins within the mitochondrial TCA cycle—the very metabolic nodes covered by the co-enriched pathways [41, 42]. We therefore postulate that the risk score may not merely reflect tumor cell proliferative activity but may also, to a considerable extent, capture intrinsic differences in cuproptosis susceptibility among HCC cells. Specifically, patients in the high-risk group may exhibit mitochondrial metabolic reprogramming driven by dysregulation of key pathway genes (e.g., DLAT and PDHA1), potentially conferring enhanced resistance to cuproptosis and ultimately manifesting as poorer clinical outcomes. These findings delineate a clear direction for future mechanistic exploration of how the signature genes cooperatively regulate cuproptosis signaling and influence HCC malignant phenotypes.

Given the potential of cuproptosis to induce immunogenic cell death, we further

investigated the relationship between the signature genes and the HCC tumor immune microenvironment (TME) [43-45] . Correlation analyses demonstrated that expression levels of CDKN2A, DLAT, MTF1, and PDHA1 were all significantly positively correlated with the infiltration abundance of B cells, $CD8^+$ T cells, $CD4^+$ T cells, macrophages, neutrophils, and dendritic cells, suggesting an “immune-hot” phenotype within tumors of high-risk patients. However, this immune-hot status did not translate into favorable clinical outcomes; rather, it was associated with poorer survival. Subsequent correlation analyses revealed significant positive associations between the four genes and immune checkpoint molecules, including CD274, HAVCR2, and PDCD1LG2. We hypothesize that this “hot but dysfunctional” immune state may stem from profound immune exhaustion and suppression in HCC, high-level $CD8^+$ T cell infiltration accompanied by upregulated checkpoints such as PD-L1 often signifies T-cell exhaustion rather than effective activation, rendering infiltrating T cells bystanders incapable of mounting effective anti-tumor responses, and potentially even facilitating an immunosuppressive microenvironment through recruitment of myeloid-derived suppressor cells. Notably, the strong correlation between cuproptosis-related gene expression and immune checkpoints suggests that this prognostic model may also hold value in predicting immunotherapy responses: high-risk patients, characterized by elevated PD-L1 expression, may exhibit enhanced responsiveness to existing immune checkpoint inhibitors, yet may require combination with cuproptosis inducers to remodel the TME and reinvigorate functional T-cell responses. This finding provides a theoretical rationale and biomarker-guided patient stratification framework for future exploration of combinatorial strategies integrating cuproptosis inducers with immune checkpoint inhibitors in HCC.

We also explored the potential epigenetic mechanisms underlying differential expression of the four genes. Promoter methylation analysis revealed that DLAT and MTF1 exhibited significantly lower methylation levels in HCC compared with normal controls, consistent with their transcriptional upregulation and suggesting that demethylation-mediated epigenetic activation may contribute to their overexpression. In contrast, CDKN2A displayed promoter hypermethylation in HCC, paradoxically accompanied by elevated mRNA expression—a phenomenon that, combined with its relatively high frequency of truncating mutations, implies that its upregulation is unlikely driven by methylation changes but may instead involve alternative mechanisms such as mutant transcript stabilization or dominant-negative effects. PDHA1 showed no significant difference in promoter methylation between tumor and normal tissues despite its marked upregulation, further indicating that its regulation likely operates through non-epigenetic pathways. Collectively, these results underscore the substantial heterogeneity in transcriptional regulatory mechanisms underlying the four-gene signature-distinct molecular events (epigenetic demethylation, mutation-driven processes, and non-epigenetic pathways) converge on a shared pro-tumorigenic expression phenotype, highlighting the complexity of cuproptosis pathway regulation in HCC.

Drug sensitivity prediction analyses revealed that high expression of the four-gene signature was associated with increased sensitivity to NPK76-II-72-1 and resistance to PD-0332991、Nutlin-3a and TGX221 in the GDSC database ($|R| > 0.2$, $P < 0.05$), while in the CTRP database, it correlated with enhanced sensitivity to 12 compounds ($|R| >$

0.15, P < 0.05). Notably, no overlap was observed between the two databases' predicted drug panels, and cytarabine showed discordant predictions—resistance in GDSC versus sensitivity in CTRP (as cytarabine hydrochloride)—highlighting that differences in screening platforms may affect predictive consistency and warranting experimental validation. Nevertheless, the broad-spectrum drug sensitivity associations exhibited by this signature offer preliminary clues regarding its potential clinical utility in guiding therapy: high-risk patients may be sensitive to multiple targeted agents while displaying intrinsic resistance to certain conventional chemotherapeutics, suggesting that clinical decision-making should integrate both risk stratification and drug sensitivity profiling.

To further delineate the specific functions of the four cuproptosis-related genes, we performed virtual knockout experiments to assess their respective roles in HCC.(Combinatorial virtual-knockout results indicate that these genes cooperatively govern metabolic homeostasis in HCC. Furthermore, the upregulation of genes involved in immunoglobulin production and B-cell activation, coupled with the repression of hepatocyte metabolic genes following perturbation, suggests that these genes may drive hepatocellular carcinoma tumorigenesis, progression and immune evasion through remodelling of the HCC tumor microenvironment.)

Moreover, the prognostic value of the four-gene signature was reproducible in an independent RNA-sequencing cohort of HCC (ICGC-LIRI-JP, n = 203). Applying the original coefficients, patients classified as high risk had significantly shorter OS than those at low risk (log-rank P = 0.0002), with a 4.01-fold increased risk of death (HR = 4.01, 95% CI 1.81–8.88, P = 0.0006) that persisted after adjustment for age, sex, and T stage (HR = 4.51, 95% CI 1.57–12.97, P = 0.005). Discriminative ability was moderate (time-dependent AUCs of 0.637 and 0.749 at 12 and 36 months, respectively; C-index = 0.687); nevertheless, the effect direction was consistent across 1,000 bootstrap resamples and the proportional-hazards assumption was satisfied (P = 0.959), supporting the robustness of the model. However, Several limitations should be acknowledged. First, the validation cohort comprised 35 death events, which limits the precision of the effect estimate and the number of covariates that can be accommodated in the multivariable model. Second, validation was performed in a single independent cohort; further validation in additional independent cohorts is warranted.

In summary, this study systematically investigates the expression landscape, prognostic value, immune associations, epigenetic regulatory mechanisms, and drug sensitivity features of cuproptosis-related genes in HCC, and successfully constructs and validates a four-gene prognostic risk model comprising CDKN2A, DLAT, MTF1, and PDHA1. This signature demonstrates potential utility in risk stratification, immune microenvironment remodeling, and drug response prediction, offering new perspectives for individualized diagnosis and treatment of HCC.

5 Conclusion

In this study, we systematically profiled the expression of cuproptosis-related genes in HCC using TCGA data and successfully constructed and validated a four-gene prognostic risk model comprising CDKN2A, DLAT, MTF1, and PDHA1. This signature effectively stratifies HCC patients into high- and low-risk subgroups, with the risk score serving as an independent prognostic factor beyond conventional clinicopathological variables. Further mechanistic exploration suggests that the model genes are closely

associated with tumor immune microenvironment remodeling, immune checkpoint regulation, and epigenetic modifications, while also demonstrating potential value in predicting drug sensitivity. The model also achieved favorable external validation results. Collectively, this four-gene prognostic model provides a novel theoretical basis and biomarker-oriented reference for individualized prognosis assessment, risk stratification, and precision therapeutic strategy development in HCC.

Acknowledgements

This work was supported by Shandong Provincial Technology Innovation Guidance Plan (No. YDZX2024063) and The Natural Science Foundation of Tianjin (No. 24JCQNJC00460).

Funding Declaration

This work was supported by Shandong Provincial Technology Innovation Guidance Plan (No. YDZX2024063) and The Natural Science Foundation of Tianjin (No. 24JCQNJC00460).

Author contributions

Study conception and design: LF, ZX and GHJ. Data curation, analysis, validation and visualization: ZX, WYH, JSL, GHJ,and LF. The draft of the manuscript: ZX, WYH, HMY, GHJ and LF. All authors reviewed the manuscript and approved the submitted version.

Data Availability declaration

The datasets in this study can be found in online repositories, and the names of the repository/repositories and accession number(s) can be found in the article/Supplementary Material.

Human Ethics and Consent to Participate declarations

Not applicable

Declaration of interest statement

The authors declare that they have no conflict of interest.

References

1. Collaboration GBoDC. Cancer Incidence, Mortality, Years of Life Lost, Years Lived With Disability, and Disability-Adjusted Life Years for 29 Cancer Groups From 2010 to 2019: A Systematic Analysis for the Global Burden of Disease Study 2019. JAMA Oncology. 2022;8(3):420–44.
2. Tan EY, Danpanichkul P, Yong JN, Yu Z, Tan DJH, Lim WH, et al. Liver cancer in 2021: Global Burden of Disease study. Journal of Hepatology. 2025;82(5):851–60.
3. European Association for the Study of the L, Sangro B, Argemi J, Ronot M, Paradis V, Meyer T, et al. EASL Clinical Practice Guidelines on the management of hepatocellular carcinoma. Journal of Hepatology. 2025;82(2):315–74.
4. Zhou J, Sun H, Wang Z, Cong W, Zeng M, Zhou W, et al. China Liver Cancer Guidelines for the Diagnosis and Treatment of Hepatocellular Carcinoma (2024 Edition). Liver Cancer. 2025;14(6):779–835.

5. Xiang D, Liu J, Wang Y, Hu D, Zhang C, Zeng T, et al. Oncofetal MCB1 Is a Functional Biomarker for HCC Personalized Therapy. Advanced Science. 2024;11(45):2401228.
6. Tsvetkov P, Coy S, Petrova B, Dreishpoon M, Verma A, Abdusamad M, et al. Copper induces cell death by targeting lipoylated TCA cycle proteins. Science. 2022;375(6586):1254–61.
7. Zhong C-C, Zhao T, Hogstrand C, Song C-C, Zito E, Tan X-Y, et al. Copper induces liver lipotoxicity disease by up-regulating Nrf2 expression via the activation of MTF-1 and inhibition of SP1/Fyn pathway. Biochimica et Biophysica Acta (BBA) - Molecular Basis of Disease. 2023;1869(6):166752.
8. Xie J, Yang Y, Gao Y, He J. Cuproptosis: mechanisms and links with cancers. Molecular Cancer. 2023;22(1):46.
9. Peng H, Zou Z, Xiang Z, Lu X, Zhang Y, Peng X. Cuproptosis-related prognostic signatures predict the prognosis and immunotherapy in HCC patients. Medicine (Baltimore). 2023;102(34):e34741.
10. Li Y, Zeng X. A novel cuproptosis-related prognostic gene signature and validation of differential expression in hepatocellular carcinoma. Frontiers in Pharmacology. 2023;Volume 13 - 2022.
11. Zhao X, Chen J, Yin S, Shi J, Zheng M, He C, et al. The expression of cuproptosis-related genes in hepatocellular carcinoma and their relationships with prognosis. Front Oncol. 2022;12:992468.
12. Smyth GK, Michaud J, Scott HS. Use of within-array replicate spots for assessing differential expression in microarray experiments. Bioinformatics. 2005;21(9):2067–75.
13. Tang Z, Li C, Kang B, Gao G, Li C, Zhang Z. GEPIA: a web server for cancer and normal gene expression profiling and interactive analyses. Nucleic Acids Res. 2017;45(W1):W98–w102.
14. Friedman J, Hastie T, Tibshirani R. Regularization Paths for Generalized Linear Models via Coordinate Descent. J Stat Softw. 2010;33(1):1–22.
15. Calcagno V, de Mazancourt C. glmulti: An R Package for Easy Automated Model Selection with (Generalized) Linear Models. Journal of Statistical Software. 2010;34(12):1 – 29.
16. Cerami E, Gao J, Dogrusoz U, Gross BE, Sumer SO, Aksoy BA, et al. The cBio cancer genomics portal: an open platform for exploring multidimensional cancer genomics data. Cancer Discov. 2012;2(5):401–4.
17. Chandrashekar DS, Bashel B, Balasubramanya SAH, Creighton CJ, Ponce-Rodriguez I, Chakravarthi BVSK, et al. UALCAN: A Portal for Facilitating Tumor Subgroup Gene Expression and Survival Analyses. Neoplasia. 2017;19(8):649–58.
18. Szklarczyk D, Gable AL, Lyon D, Junge A, Wyder S, Huerta-Cepas J, et al. STRING v11: protein–protein association networks with increased coverage, supporting functional discovery in genome-wide experimental datasets. Nucleic Acids Research. 2019;47(D1):D607–D13.
19. Li T, Fu J, Zeng Z, Cohen D, Li J, Chen Q, et al. TIMER2.0 for analysis of tumor-infiltrating immune cells. Nucleic Acids Research. 2020;48(W1):W509–W14.
20. Han Y, Wang Y, Dong X, Sun D, Liu Z, Yue J, et al. TISCH2: expanded datasets and new tools for single-cell transcriptome analyses of the tumor microenvironment. Nucleic Acids Research. 2023;51(D1):D1425–D31.

21. Osorio D, Zhong Y, Li G, Xu Q, Yang Y, Tian Y, et al. scTenifoldKnk: An efficient virtual knockout tool for gene function predictions via single-cell gene regulatory network perturbation. Patterns. 2022;3(3):100434.
22. Totoki Y, Tatsuno K, Covington KR, Ueda H, Creighton CJ, Kato M, et al. Trans-ancestry mutational landscape of hepatocellular carcinoma genomes. Nature Genetics. 2014;46(12):1267–73.
23. Lian Q, Wang S, Zhang G, Wang D, Luo G, Tang J, et al. HCCDB: A Database of Hepatocellular Carcinoma Expression Atlas. Genomics, Proteomics & Bioinformatics. 2018;16(4):269–75.
24. Yin Q, Yao Y, Ni J, Zhang Y, Wu J, Zeng H, et al. DLAT activates EMT to promote HCC metastasis by regulating GLUT1-mediated aerobic glycolysis. Mol Med. 2025;31(1):71.
25. Zhang P, Zhao JH, Yuan LX, Ju LL, Wang HX, Wang F, et al. DLAT is a promising prognostic marker and therapeutic target for hepatocellular carcinoma: a comprehensive study based on public databases. Sci Rep. 2023;13(1):17295.
26. Shao K, Shen H, Chen X, Shao Z, Liu Y, Wang Y, et al. Copper transporter gene ATP7A: A predictive biomarker for immunotherapy and targeted therapy in hepatocellular carcinoma. Int Immunopharmacol. 2023;114:109518.
27. Iseda N, Itoh S, Yoshizumi T, Tomiyama T, Morinaga A, Yugawa K, et al. Impact of Nuclear Factor Erythroid 2-Related Factor 2 in Hepatocellular Carcinoma: Cancer Metabolism and Immune Status. Hepatol Commun. 2022;6(4):665–78.
28. Leung HW, Lau EYT, Leung CON, Lei MML, Mok EHK, Ma VWS, et al. NRF2/SHH signaling cascade promotes tumor-initiating cell lineage and drug resistance in hepatocellular carcinoma. Cancer Letters. 2020;476:48–56.
29. Lee K, Kim S, Lee Y, Lee H, Lee Y, Park H, et al. The Clinicopathological and Prognostic Significance of Nrf2 and Keap1 Expression in Hepatocellular Carcinoma. Cancers [Internet]. 2020; 12(8):[2128 p.].
30. Sun B, Ding P, Song Y, Zhou J, Chen X, Peng C, et al. FDX1 downregulation activates mitophagy and the PI3K/AKT signaling pathway to promote hepatocellular carcinoma progression by inducing ROS production. Redox Biol. 2024;75:103302.
31. Wang W, Lu K, Jiang X, Wei Q, Zhu L, Wang X, et al. Ferroptosis inducers enhanced cuproptosis induced by copper ionophores in primary liver cancer. J Exp Clin Cancer Res. 2023;42(1):142.
32. Zhang P, Zhou C, Ren X, Jing Q, Gao Y, Yang C, et al. Inhibiting the compensatory elevation of xCT collaborates with disulfiram/copper-induced GSH consumption for cascade ferroptosis and cuproptosis. Redox Biology. 2024;69:103007.
33. Yan C, Niu Y, Ma L, Tian L, Ma J. System analysis based on the cuproptosis-related genes identifies LIPT1 as a novel therapy target for liver hepatocellular carcinoma. Journal of Translational Medicine. 2022;20(1):452.
34. Ding J, Guo P, Deng Y-T, Deng Y, Chen K-Y, Han F. CDKN2A as a prognostic and diagnostic marker is a possible key contributor in hepatocellular carcinoma. Translational Cancer Research. 2025;14(4):2303–18.
35. Yang W, Nguyen R, Safri F, Xu Y, Zhou Y, Bao J-F, et al. CDKN2A alterations as possible molecular link between environmental pollutants and pathogenesis of liver cancer: Epidemiology, mechanisms, and insights. Hepatobiliary & Pancreatic Diseases International. 2026.

36. Wang N, Lu S, Cao Z, Li H, Xu J, Zhou Q, et al. Pyruvate metabolism enzyme DLAT promotes tumorigenesis by suppressing leucine catabolism. Cell Metabolism. 2025;37(6):1381–99.e9.
37. Song L, Zeng R, Yang K, Liu W, Xu Z, Kang F. The biological significance of cuproptosis-key gene MTF1 in pan-cancer and its inhibitory effects on ROS-mediated cell death of liver hepatocellular carcinoma. Discov Oncol. 2023;14(1):113.
38. Yang Y, Qian Cai Q, Sheng Fu L, Wei Dong Y, Fan F, Zhong Wu X. Reduced N6-Methyladenosine Mediated by METTL3 Acetylation Promotes MTF1 Expression and Hepatocellular Carcinoma Cell Growth. Chem Biodivers. 2022;19(11):e202200333.
39. Lu L, Ma Y, Lu Y, Luo Z, Zhao Z, Ma J, et al. PDHA1 Orchestrates Hepatocellular Carcinoma Progression Through LINC00607-Mediated Regulation of Cuproptosis and Immune Evasion. Digestive Diseases and Sciences. 2025;70(11):3730–42.
40. Pan Y, Zhang Y, Mao D, Fang Z, Ma Y, Jin D, et al. Multi-omics Insights into PDHA1 as a Predictive Biomarker for Prognosis, Immunotherapy Efficacy, and Drug Sensitivity in Hepatocellular Carcinoma. ACS Omega. 2024;9(46):46492–504.
41. Chen H, Zhou Z, Tu Y, Yang Y, Liu X, Phoeurm N, et al. Copper homeostasis and cuproptosis: molecular mechanisms and therapeutic opportunities. Molecular Biomedicine. 2026;7(1):107.
42. Li S-R, Bu L-L, Cai L. Cuproptosis: lipoylated TCA cycle proteins-mediated novel cell death pathway. Signal Transduction and Targeted Therapy. 2022;7(1):158.
43. Guo K, Wang T, Yin J, Yang S, Cui H, Cao Z, et al. Identification of Cuproptosis-Related Patterns Predict Prognosis and Immunotherapy Response in Hepatocellular Carcinoma. J Cell Mol Med. 2024;28(23):e70224.
44. Lei G, Lu Z, Xu Z, Braun C, Huo D, Gao J, et al. Cuproptosis-immunity crosstalk informs strategy to overcome immunotherapy resistance. Cell. 2026.
45. Yun K, Yu X, Liang S, Wang Q, Zhang Z, Han Y, et al. Tumor-responsive cuproptosis nanoinducer realizing efficient PANoptosis for enhanced cancer immunotherapy. Theranostics. 2025;15(17):9294–305.

Figure legends

Figure S1. Mutational landscape of the four cuproptosis-related genes in HCC. Oncoprint visualization of somatic mutation frequencies and alteration types for CDKN2A, DLAT, MTF1, and PDHA1 in HCC samples from the TCGA database via cBioPortal. The panel shows the overall mutation frequency (%) for each gene. Mutation types are color-coded as indicated in the legend.

Figure S2. Associations between the four-gene signature and immune checkpoint expression in HCC. Correlation scatter plots of CDKN2A, DLAT, MTF1, and PDHA1 with CTLA4, HAVCR2, PDCD1, TIGIT, CD274, LAG3, SIGLEC15, and PDCD1LG2 in HCC based on the TIMER 2.0 database. Spearman correlation coefficients and P-values are shown. $P < 0.05$ was considered statistically significant.

Table S1. GDSC dataset analysis for the correlations between the four-gene signature expression and drug sensitivity profiles.

Table S2. CTRP dataset analysis for the correlations between the four-gene signature expression and drug sensitivity profiles.

Supplementary Files

This is a list of supplementary files associated with this preprint. Click to download.

- TableS2CtrpDrugIC50AndExpTable.xlsx
- TableS1GdscIC50AndExprTable.xlsx
- FigureS1.tif
- FigureS2.tif